Simulation Study of Rectifying Antenna Structure for Infrared Wave Energy Harvesting Applications

Xi Shao[1,2], N. Goldsman[1,2], N. Dhar[3], F. Yesilkoy[1], A. Akturk[1,2], S. Potbhare[1,2], M. Peckerar[1]

1. Department of Electrical and Computer Engineering, University of Maryland, College Park, MD 20742, USA, xshao@umd.edu
2. CoolCAD Electronics LLC, 5000 College Ave. College Park, MD 20740, USA
3. Defense Advanced Research Projects Agency, Microsystems Technology Office, Arlington, VA 2220

Abstract— **We present an integrated modeling of an infrared energy harvesting rectenna, which is the integrated combination of a micron size antenna and a nano-scale tunneling diode. The computational model consists of a 2D electrical potential solver in polar coordinate with adaptive gridding to ensure the finest resolution around the antenna tip and a transmission matrix-based Schrodinger equation solver for calculating the electron tunneling probability through the junction. The numerical model enables us to study the rectifying nature of the rectenna and performed scaling analysis of the electron emission from rectifying antenna structure.**

Keywords-infrared energy harvesting; tunneling diode; rectifying antenna

I. INTRODUCTION

There are several major radiation sources having wavelengths in the infrared range on the surface of Earth: direct solar radiation and heat-bodies. The solar radiation in these infrared spectra can amount to ~100 W/m^2. Another major source of infrared radiation on the surface of the Earth is the heat-bodies, e.g. human bodies of temperature around 300 K, Earth's ground and other heat sources with high temperature. These heat-bodies emit significant amount of infrared radiation, e.g. with peak radiation at wavelengths 9.6 um for objects with temperature 300 K. On the other hand, existing solar cell materials can absorb radiation with wavelengths upto 1.2 um in a relatively efficient way (with efficiency 10-18%). But, there are no existing efficient ways to harvest infrared radiation for wavelengths from 1.25 um to 10 um.

Recently a number of developments in nano-antenna design and fabrication [1] have taken place. These developments are of industrial significance and motivate us to develop models to investigate a promising infrared energy-harvester structure: rectenna. A rectenna is formed with a thin layer of metallic triangle with a sharp tip placed next to a layer of metallic rectangle on top of a substrate. The rectenna is designed to harvest energy by rectifying infrared electromagnetic wave through tunneling diode structure formed with the metallic tip-rectangle junction. The sharp tip of the triangle patch will focus and enhance the electric field under radiation so that it is high enough to enable electrons to tunnel through the junction [2]. To quantify the performance of rectenna energy harvester, we developed an integrated modeling tool to solve for electric potential field distribution around the tip-rectangle junction and use the spatial electric field configuration to feed to Schrodinger equation solver to calculate electric field emission under forward and reverse-bias configurations. The model enables us to quantitatively evaluate the dependence of the electron emission efficiency on the various designs of the rectenna such as antenna tip sharpness, gap distances, etc.

II. SIMULATION MODEL

A. Simulation Geomatry

The rectenna structure is modeled in polar coordinates. Fig. 1 shows the zoom-in view of grid configuration in which grids with radially adaptive gridding are employed to ensure the finest resolution around the metal tip. The simulation domain spans from $\theta = -\theta_0$ to $\theta = \theta_0$ azimuthally and the azimuthal boundary is located at $\theta = \pm\theta_0$ with the angular span of the sharp tip being $2\theta_0$. The metallic nature of the sharp tip is prescribed as the boundary condition at $\theta = \pm\theta_0$ in the simulation. In total, 300 uniformly-spaced grids are used azimuthally and 400 non-uniformly-spaced grids are used radially with the finest resolution = 0.1 nm around the tip.

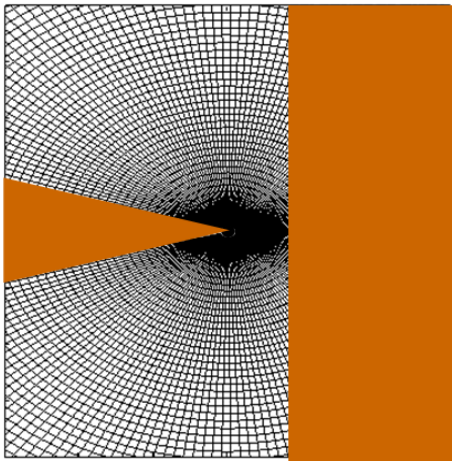

Fig. 1: Structure of rectenna and zoom-in view of simulation grid configuration.

ISBN 978-0-615-71756-2

B. Electric Potential Solver

The electric potential field $\Phi(r,\theta)$ within the gap between the metallic sharp tip and rectangular patch can be obtained by solving the Poisson's equation:

$$\nabla^2\Phi(r,\theta) = -\frac{\rho}{\varepsilon}, \qquad (1)$$

where ρ is the charge density and ε is the permittivity of the medium. In our case, the charge density $\rho = 0$ within the gap region and the potential field in polar coordinate satisfies

$$\frac{\partial^2\Phi}{\partial r^2} + \frac{1}{r}\frac{\partial\Phi}{\partial r} + \frac{1}{r^2}\frac{\partial^2\Phi}{\partial\theta^2} = 0. \qquad (2)$$

Eq. (2) is discretized onto the polar coordinates (r_i,θ_j) (see Fig. 1) with $i = 1,\ldots, n_r$ and $j = 1,\ldots, n_\theta$. The boundary conditions for $\Phi(r,\theta)$ satisfies the biasing potential difference between the metallic sharp tip and rectangle patch. For a sharp tip, the boundary condition is specified as $\Phi(r_i,\theta_1) = \Phi(r_i,\theta_{n_\theta}) = V_1$. For the rectangle patch, the boundary condition is specified as $\Phi(r_i,\theta_j) = V_2$ for (r_i,θ_j) satisfying $r_i\cos(\theta_j) > d$, where d is the gap distance between the sharp tip and rectangle patch. To solve for the potential field configuration fromEq. (2), it requires the inversion of a block diagonal matrix and we used sparse matrix algebra to obtain the solution.

C. Electron Tranmission Calculation

Using the numerically obtained 2D potential field distribution $\Phi(r,\theta)$, we can calculate the electron tunneling probability through the junction by solving the Schrodinger equation. The time-independent Schrodinger equation across the gap can be written as

$$\nabla^2\Psi(r,\theta) + \frac{8\pi^2 m}{h^2}(E - \Phi(r,\theta))\Psi(r,\theta) = 0, \qquad (3)$$

where $\Psi(r,\theta)$ is electron wave-function, m is the electron mass, E is the electron energy. To calculate the tunneling probability, we approximate the potential barrier as in one dimension along radial direction for each discrete azimuthal angle $\theta = \theta_j$, and Eq. (3) can be approximated as

$$\frac{d^2\Psi(r,\theta)}{dr^2} + \frac{8\pi^2 m}{h^2}(E - \Phi(r,\theta))\Psi(r,\theta) = 0. \qquad (4)$$

By doing so, we have neglected the $1/r^2$ term as compared to other energy terms. Such kind of approximation was used and justified in [3, 4] for solution of electron emission from sharp spherical and cylindrical surfaces.

A variety of approximate and numerical techniques for solving the Schrodinger equation were developed [5–8]. We adopted the transmission matrix-based approach developed by *Ando and Itoh* [6] to numerically solve Eq. (4). The numerical scheme can calculate the electron transmission coefficient and current across arbitrary potential barriers. In this method, multistep potential approximation is used to approximate variations of potential energy and electron effective mass. The final transmission coefficient is calculated by connecting momentum eigen-functions. This method is briefly summarized as follows. The discretize wave function $\Psi_i(r)$ in the *i*th region along *r* for an electron with energy *E* can be expressed as

$$\Psi_i(r) = A_i\exp(ik_i r) + B_i\exp(-ik_i r). \qquad (5)$$

From continuity of wave function and its first derivative, the wave amplitude (A_i , B_i) in the *i*th region can be obtained with

$$\begin{pmatrix} A_i \\ B_i \end{pmatrix} = \prod_{l=1}^{i-1} M_l \begin{pmatrix} A_0 \\ B_0 \end{pmatrix} = M\begin{pmatrix} A_0 \\ B_0 \end{pmatrix}, \qquad (6)$$

where M_l is the transmission matrix for *l*th region and its detailed form can be found in [6]. By setting $A_0 = 1$ and $B_{n_r} = 0$, we can obtain the transmission amplitude A_{n_r} and thus determine the electron transmission probability.

III. Simulation Results

A. Electric Potential Field Distribution of Rectanna

Fig. 2 shows the numerical solution of potential field configurations obtained for forward-biased rectennas of different tip angles and gap distances. The sharp metal tip is negatively biased. The solution is able to resolve the sharp potential change around the tip and across the narrow gap with the spatial resolution varying from sub nanometer to sub-micron. This is made possible through the adaptive gridding we used in the radial direction.

B. Scaling of ElectricFfield Enhancement

Fig. 3a and 3c shows the dependence of the potential field distribution along the $\theta = 0$ axis across the gap on the gap distance and conical angle of the metal tip. The electric potential changes sharply when the gap distance shrinks. With the potential field solution, we are able to calculate the electric field which is responsible for the electron emission and further derive the electric field enhancement factor. The electric field enhancement factor is defined as relative to the incident electric field amplitude illuminating on a rectanna with a triangular patch of 2.5 um height (one quarter of the 10 um IR wavelength). Fig. 3b and 3d shows the dependence of the peak electric field enhancement factor on the gap dependence and antenna tip angle. In general, the peak electric field within the gap depends strongly on the gap distance and the field is stronger with a sharper tip and narrower gap.

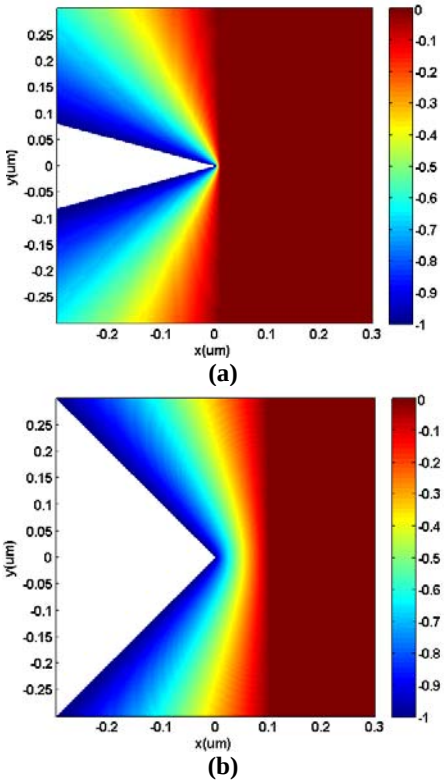

Fig. 2: Simulated potential field configuration for forward-bias rectennas with (a) tip angle = 30 deg. and gap distance = 10 nm, and (b) tip angle = 90 deg. and gap distance = 100 nm.

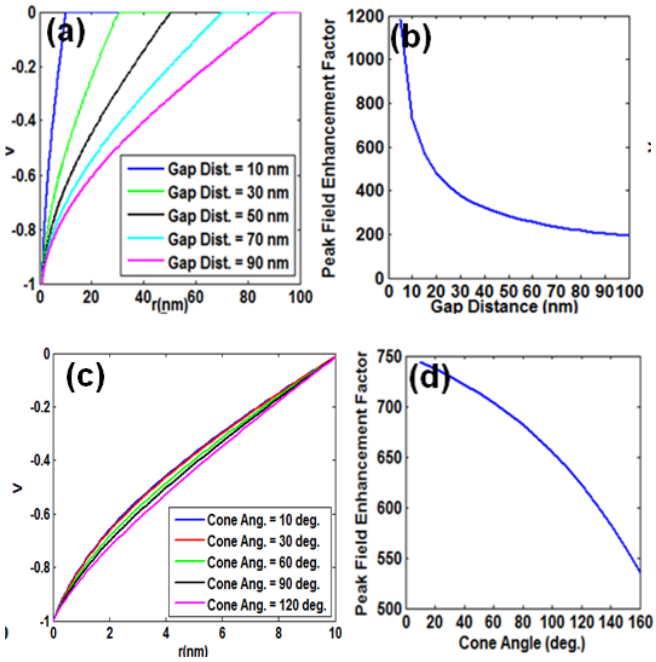

Fig. 3: (a, c) Voltage distribution along *x* for different gap distances and cone angles, respectively. (b, d) Peak electric field enhancement factor within the gap vs. gap distance and cone angle, respectively. (a, b) tip angle = 30 deg; (c, d) gap distance = 10 nm.

C. Illustration of the Rectifying Nature of the Rectenna

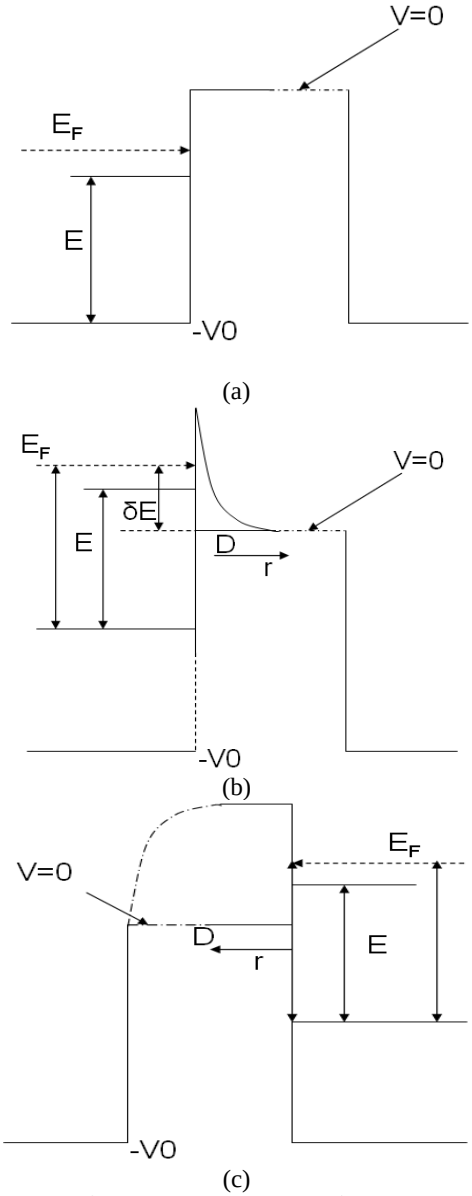

Fig. 4: Illustration of electron potential energy configuration over the gap for rectenna under (a) floating (b) forward (barrier width varies from 0.6 to 2.4 nm) and (c) reverse bias.

We first use Fig. 4 to schematically illustrate the rectifying nature of the rectenna. Fig. 4a shows the potential energy of electron over the gap of potential barrier V_0 for a floating rectenna without illumination of IR radiation. With forward-bias, the potential energy of electron across the gap is shown in Figure 4b. Under forward bias, the potential field changes sharply away from the tip and the effective barrier is narrow. It is easier for the electron to tunnel through the barrier and produce emission [2]. Under reverse-bias as shown in Fig. 4c, the potential field changes gradually away from the rectangle patch and the effective barrier is wide. Therefore the electron

emission is harder. These asymmetric aspects in the electron tunneling under forward and reverse-bias are further quantified in next section.

D. Electron Tunneling Probability Calculation

We next use the Schrodinger equation solver to calculate the electron tunneling probability through the junction with the calculated 2D electric potential field distribution for various configurations of forward and reverse-bias rectennas.

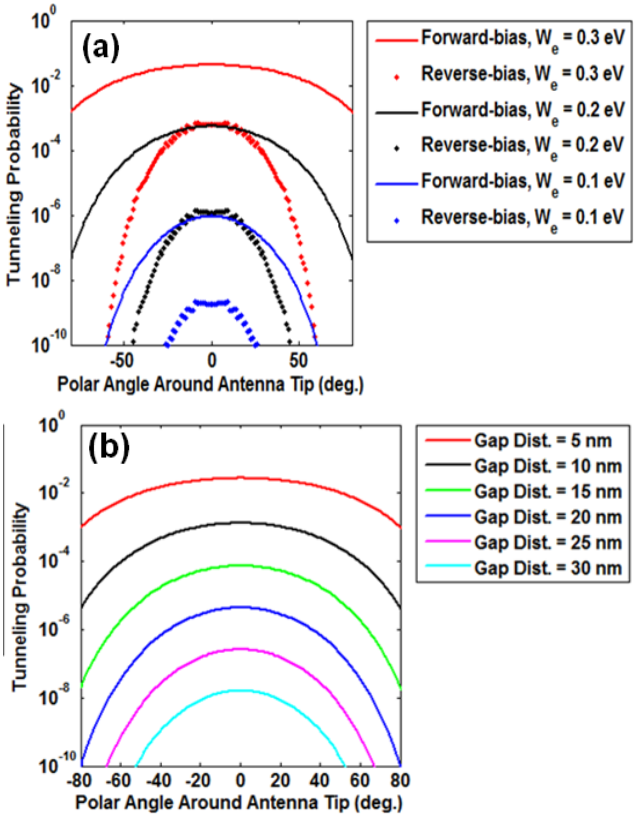

Fig. 5: (a) Electron tunneling probability of selected electron energies vs. polar angle around the antenna tip for forward and reverse-biased rectenna. Gap distance = 5 nm. (b) Electron tunneling probability for electron of energy 0.2 eV *vs.* polar angle at forward-bias for rectenna of different gap distances. For (a) and (b), antenna tip conical angle = 30 deg and electric potential barrier height = 0.4 V.

Fig. 5a shows the calculated electron tunneling probability vs. polar angle around the rectenna tip for forward and reverse-bias configuration. The conical angle of antenna tip is 30 degrees and potential barrier height is 0.4 V. It can be seen that the tunneling probability under forward-bias is orders of magnitude higher than under reverse-bias. For a rectenna with 5 nm gap distance under forward bias, the barrier width around the tip is 0.6, 1.4, and 2.4 nm for electron of energy 0.1, 0.2, and 0.3 eV below the barrier, respectively, which explains the high tunneling probability. Under forward-bias, tunneling probability is high over a much wider range of polar angle around the tip. The asymmetric geometry of the rectenna enables directional tunneling of electrons and the sharp tip field enhancement further enhances the directional tunneling. Therefore, the rectenna can effectively rectify electron current and harvest infrared energy. Fig. 5b shows the electron tunneling probability for electron of energy 0.2 eV *vs.* polar angle for rectenna of different gap distances. In general, the tunneling probability increases sharply with the decreasing gap distance.

IV. SUMMARY

In summary, an integrated numerical model was developed to investigate the electron emission from rectifying antenna structure. The model consists of a 2D electrical potential solver with adaptive gridding to have the finest resolution around the antenna tip and a transmission matrix-based Schrodinger equation solver for calculating the electron tunneling probability. In general, we strive for smaller gap distance, sharper metallic antenna tip angle and lower barrier height to increase tunneling probability and tunneling current. But it is also important to consider that the gap distance can't be too small so that the capacitance is not exceptionally large to have large RC constant and diminish the rectifying ability. The rectenna shown in this paper can also be used for infrared wave detection applications.

REFERENCES

[1] Sundaramurthy, A., P. James Schuck, Nicholas R. Conley, David P. Fromm, Gordon S. Kino, and W. E. Moerner, Toward Nanometer-Scale Optical Photolithography: Utilizing the Near-Field of Bowtie Optical Nanoantennas, *Nano Letters*, Vol. 6, No. 3, 355-360, 2006.

[2] R. Fowler and L. Nordheim, Electron Emission in Intense Electric Fields Proc. R. Soc. London, Ser. A **119**, 173, 1928.

[3] M. S. Sodha and A. Dixit, A critical look at electric field emission of electrons from metallic surfaces, J. Appl. Phys. **104**, 064909, 2008.

[4] M. S. Sodha and A. Dixit, Effect of Debye shielding on electric field emission from spherical and cylindrical surfaces, *J. Appl. Phys*. **105**, 034909, 2009.

[5] Roy S, Ghatak A K, Goyal I C and Gallawa R L 1993 Modified Airy function method for the analysis of tunneling problems in optical waveguides and quantum-well structures *IEEE J. Quantum Electron.* **29** 340–34.

[6] Ando, Yuji, and Tomohiro Itoh, Calculation of transmission tunneling current across arbitrary potential barriers, *J. Appl. Phys.*, 61 (4), 1987.

[7] Ghatak A K, Gallawa R L and Gayal I C 1992 Accurate solutions to Schr¨odinger's equation using modified Airy functions *IEEE J. Quantum Electron.* **28** 400–3.

[8] Nakamura K, Shimizu A and Koshiba M 1991 Finite-element calculation of the transmission probability and the resonant-tunneling lifetime through arbitrary potential barriers *IEEE J. Quantum Electron.* **27** 1189–98.